Ferroelectric PVDF nanofiber membrane for high-efficiency PM0.3 air filtration with low air flow resistance

Tan Tan Bui [a], Min Kyoung Shin [b], Seung Yong Jee [c], Dang Xuan Long [b,d], Jongin Hong [b,d,*], Myung-Gil Kim [a,**]

[a] School of Advanced Materials Science and Engineering, Sungkyunkwan University, Suwon 16419, Republic of Korea
[b] Department of Chemistry, Chung-Ang University, Seoul 06974, Republic of Korea
[c] Lemon Corporation, Gumi 39170, Republic of Korea
[d] Department of Smart Cities, Chung-Ang University, Seoul 06974, Republic of Korea

GRAPHICAL ABSTRACT
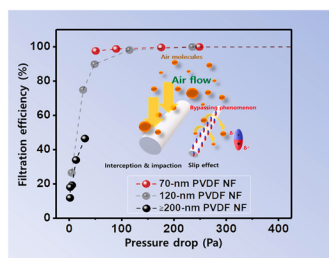
ARTICLE INFO

ABSTRACT

The significant public health concerns related to particulate matter (PM) air pollutants and the airborne transmission of severe acute respiratory syndrome coronavirus 2 (SARS-CoV-2) have led to considerable interest in high-performance air filtration membranes. Highly ferroelectric polyvinylidene fluoride (PVDF) nanofiber (NF) filter membranes are successfully fabricated via electrospinning for high-performance low-cost air filtration. Spectroscopic and ferro-/piezoelectric analyses of PVDF NF show that a thinner PVDF NF typically forms a ferroelectric β phase with a confinement effect. A 70-nm PVDF NF membrane exhibits the highest fraction of β phase (87%) and the largest polarization behavior from piezoresponse force microscopy. An ultrathin 70-nm PVDF NF membrane exhibits a high $PM_{0.3}$ filtration efficiency of 97.40% with a low pressure drop of 51 Pa at an air flow of 5.3 cm/s owing to the synergetic combination of the slip effect and ferroelectric dipole interaction. Additionally, the 70-nm PVDF NF membrane shows excellent thermal and chemical stabilities with negligible filtration performance degradation (air filtration efficiency of 95.99% and 87.90% and pressure drop of 55 and 65 Pa, respectively) after 24 h of heating at 120 °C and 1 h immersion in isopropanol.

1. Introduction

Particulate matter (PM: $PM_{0.3}$, $PM_{2.5}$, $PM_{1.0}$) has recently emerged as a substantial global public healthcare concern with rapid urbanization and excessive fossil fuel use [1,2]. $PM_{0.3}$ (particle sizes $\leq$ 0.3 μm) is the most penetrating particle size (MPPS) by the conventional filtration method (Scheme 1a), and it is considered the most hazardous component [3–7]. $PM_{0.3}$ is a severe threat to public health because long-term exposure to these fine specks of dust can cause respiratory diseases, lead to lung cancer, and eventually, result in mortality [8–11]. Additionally, the recent severe acute respiratory syndrome coronavirus 2 (SARS-CoV-2) spreads rapidly through tiny water droplets [12,13], resulting in a massive surge in daily confirmed cases and deaths [14,15]. Therefore, urgent demands exist for air filtration to prevent the spread of SARS-CoV-2 and provide cleaner air for our respiration. The reduction of airborne PM, which may contain virus-contaminated droplets from airflow, has been critically regarded as an effective method for public health improvement. Various strategies have been proposed to remove PM from airflow; however, the simple physical membrane filtration of PM is considered to be a feasible solution to mitigate these issues [16,17].

To develop a highly efficient air filtration membrane, fibrous-web filters have been fabricated using various techniques, such as melt blown (MB), needle punched, and wet-laid processes [6,18–20]. However, these methods typically experience large-scale aperture, limited fiber diameter reduction, and severely aggregated conjunction, which results in limited air filtration performance for fine particles [21,22]. Currently, a thick MB filter that includes an electret is widely used as a PM sieving membrane. As PM passes through porous filter media, the strong electrostatic attraction of PM to filter fibers enables significant reduction in filter fiber loading and a subsequent low pressure drop with high filtration efficiency [23,24]. However, several remaining limitations require attention, including a large fibrous diameter, filtration performance loss, and non-reusability [22,25]. The filter functions are predominantly based on the electret charge effect, which is effective under limited conditions, requiring an oil- or alcohol vapor-free environment. The deterioration of electrostatic force and filter efficiency have been observed as a charge loss when the MB filter is exposed to an organic solvent, such as isopropanol, ethanol, and acetone [26–28]. Furthermore, the non-reusability of MB filters is a recent concern owing to the extensive need for masks to prevent the spread of coronavirus (COVID-19) [29]. The use of nanoporous membrane to mechanically sieve PM is emerging as an alternative strategy to overcome the limitations of MB filters that use the depth filtration mechanism [30]. However, the high pressure drop of conventional nanoporous membranes remains a critical challenge for commercialization.

The application of the slip effect to mitigate the limitations of nanoporous membrane filters has gained significant interest; it enables a lower pressure drop as air molecules bypass the mean free path (65.3 nm) over the fiber, simultaneously resulting in a high PM filtering efficiency (Scheme 1b) [1,31,32]. Therefore, an electrospun nanofibrous filter can surmount the limitations of a large-diameter electret filter. The electrospinning method enables facile nanofiber (NF) membrane fabrication with an ultrathin diameter (10–1000 nm) under a high electric field [33–35], which is considered to be an advanced physical filter that adopts the slip effect region of the air flow. Other strategies have been extensively implemented to increase the capture of fine dust, including chemical functionalization [36] and filter charging [37]. Among them is ferro/piezo-electricity, which employs a unique electroactive property with stable spontaneous polarization to efficiently
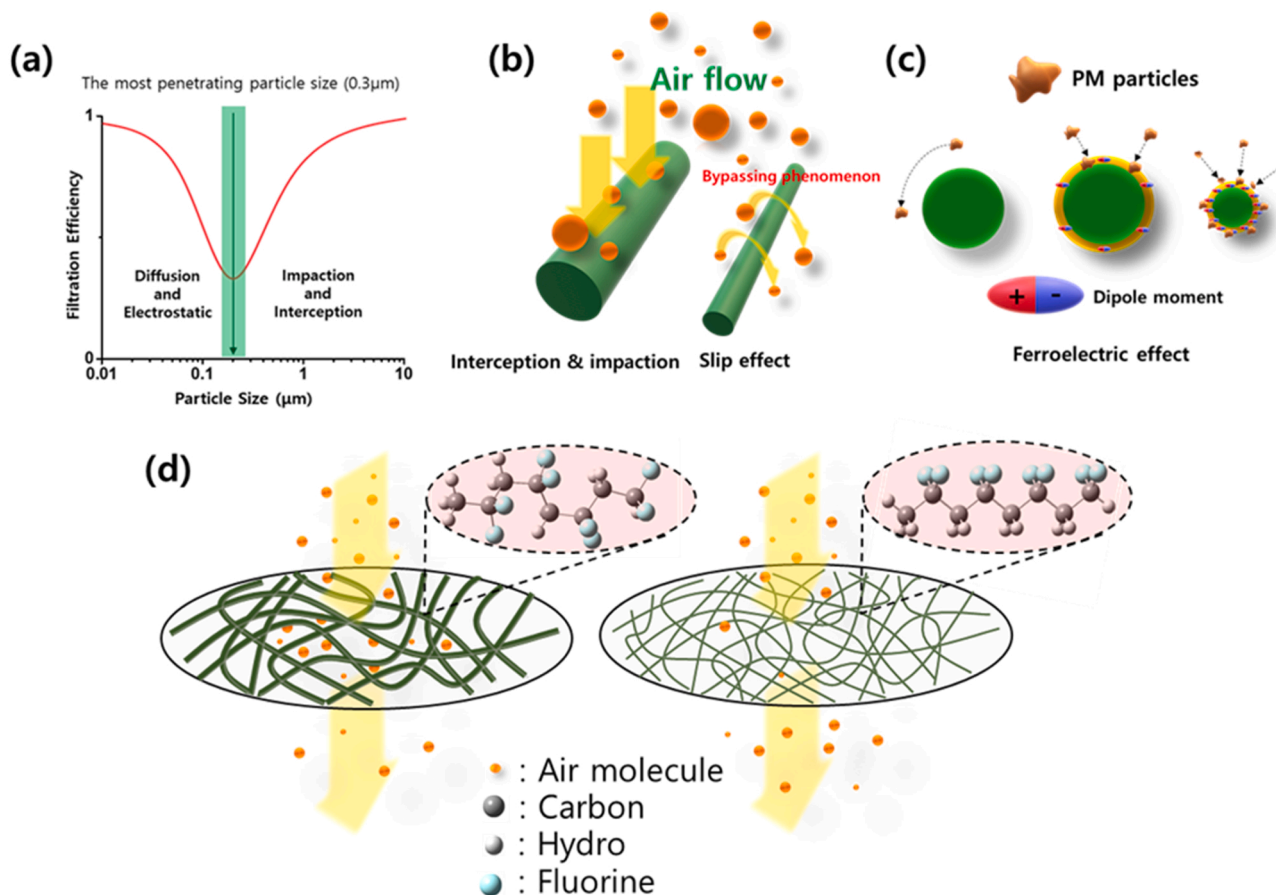
Scheme 1. Schematic illustration of PVDF NF air filter. (a) Representative curve of the MPPS (0.3 μm). (b) Emergence of the slip effect with fiber diameter variation. (c) Impact of ferroelectricity on capturing PM. (d) Phase transformation of PVDF and its effect on air filtration with different filter diameters.

trap microdust with a large built-in electric field (Scheme 1c) and prevent the inhalation of PM.

Among the diverse polymers for electrospun NFs, polyvinylidene fluoride (PVDF) has attracted substantial research attention owing to its excellent mechanical properties, good thermal stability, feasible processing, high chemical resistance and flexibility, and highly electroactive properties. PVDF consists of five possible crystalline phases, which include α, β, γ, δ, and ε [38–40]. The β phase PVDF is a well-known polar phase with excellent ferroelectric and piezoelectric properties [41,42]. However, the thermodynamically stable phase of PVDF is the non-electroactive α phase. There have been significant efforts to realize a β structure with high phase purity; however, the simple fabrication of β phase PVDF NF air filters has not yet been realized. It remains challenging to realize a high-performance filter with a robust and easily scalable NF membrane using pure β phase PVDF.

Herein, we report an electrospun high-performance PVDF NF filter membrane with self-polarized ferroelectric phase and an ultra-thin diameter. We utilized the slip effect of air molecules with nanofiber by controlling the diameter and uniformity of the electrospun PVDF NF membrane via the addition of sodium dodecyl sulfate (SDS) as a conducting surfactant. Particularly, the presence of the β phase in the 70-nm membrane results in the greatest phase polarization versus bias voltage curve characterization for the intrinsic piezo-/ferroelectricity of PVDF NF materials. The optimized 70-nm PVDF NF membrane exhibits a low pressure drop with high PM0.3 filtration efficiency (FE), and a high quality factor. Moreover, the optimized 70-nm PVDF membrane also exhibits excellent chemical and thermal stability and high retention of

air FE under isopropyl alcohol immersion and heat treatment.

2. Materials and methods

2.1. Materials

PVDF (21510 Solef) was purchased from Solvay Specialty Polymer (Belgium). N,N- dimethylacetamide (DMAc), 2-butanone (MEK), and SDS were purchased from Sigma-Aldrich (USA). All chemicals were used without further purification.

2.2. Preparation of polymer solution

PVDF powder (15 wt%) was dissolved in a mixed solvent of DMAc and MEK (DMAc:MEK = 5:5). Varying contents of SDS, from 0.05 to 0.5 wt% of the PVDF, were then added to the solution. The polymer solutions were stirred overnight at 25 °C.

2.3. Fabrication of nanofibrous membrane

PVDF nanofibers were fabricated by an electrospinning system (ESR200PR2, NanoNC Co. Ltd., South Korea). The syringe for the polymer solution was directly linked with one or five metallic spinneret needles (27 G) and was installed onto a movable supporting frame. As simply depicted in Fig. 1a, electrospinning of the PVDF solution was performed with a feed rate of 0.5 mL/h and a high DC voltage of 28 kV at the spinneret needle tip with a fixed distance of 16 cm from the
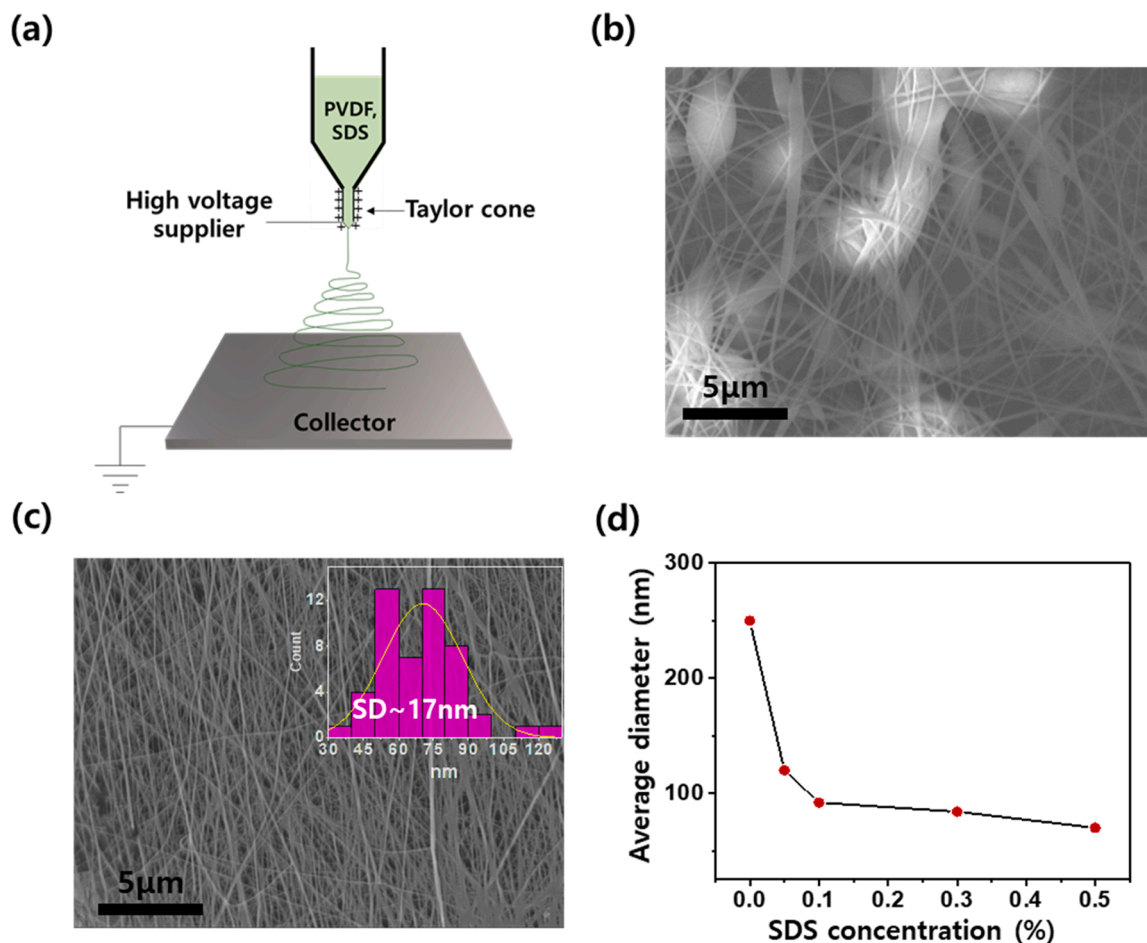
Fig. 1. Surface morphology of nanofibrous membrane at various diameters. (a) Electrospinning processing configuration of the PVDF polymer and SDS additive. FE-SEM images of (b) electrospun pristine PVDF sample and (c) 0.5 wt% SDS-containing sample. (d) Average PVDF nanofiber diameter variation with SDS concentration change.

spinneret tip to the grounded collector. The entire experiment was conducted at a humidity level of approximately 20%.

2.4. Characterization of nanofibrous membrane

The morphology of the electrospun PVDF and SDS-PVDF nanofibrous membranes was characterized using field-emission scanning electron microscopy (FE-SEM, JSM-6700 F) at the MEMS·Sensor Platform Center of SungKyunKwan University and ImageJ (National Institutes of Health and Laboratory for Optical and Computational Instrumentation, University of Wisconsin). Chemical properties of the PVDF samples were analyzed using Fourier transform infrared spectroscopy (FTIR, IFS-66/S, TENSOR27, Bruker, USA). Grazing incident X-ray diffraction (GIXRD) patterns were obtained with an X′Pert Pro (PANalytical, Netherlands) using Cu Kα radiation. A commercial atomic force microscope (AFM, XE-120, Park Systems, South Korea) connected to a lock-in amplifier (SR830, Stanford Research Systems, USA) was used to image the topography of the electrospun NFs and determine their ferroelectric properties at nanoscale. An alternating current modulated voltage of 1.5 V_{rms} with a frequency of 17 kHz was applied to a Pt/Ir-coated Si tip (PPP-EFM, Nanosensors, Switzerland), which was used as the top electrode. Piezoresponse hysteresis loops of a single PVDF NF on an Au-coated Si substrate were measured by positioning the tip on top of a selected position and monitoring the piezoresponse signal as a function of the dc bias applied to the bottom electrode. The local hysteresis loop measurement was carried out on three single nanofibers for each PVDF NF diameter. The air FE (%) and pressure drop (ΔP) of nanofibrous membranes were tested using the Automated Filter Tester 8130 (TSI, USA) with airflow of 5.3 cm/s and NaCl aerogel particles (average diameter: 0.3 μm) as simulated PM. Each obtained result was averaged by three tests. The quality factor (QF) was estimated to evaluate the overall performance of the filter membrane using Eq. (1):

$$QF = -\frac{\ln(1-\eta)}{\Delta P} \tag{1}$$

where η and ΔP are the air FE and pressure drop, respectively.

2.5. Chemical and thermal stability test of PVDF NF filter

For the chemical stability test, the filter membranes were completely immersed in IPA for various periods and subsequently dried in ambient air for 12 h. For the thermal stability test, the filter membranes were heated at different temperatures for 24 h in a vacuum oven.

3. Results and discussion

3.1. Morphology analysis of nanofibrous membrane

The reticular support structure and tortuous pore channels of nanofiber-based filters enable the effective passage of air molecules while trapping the PM. If the nanofibrous diameter is close to the mean free path length of the air molecules (65.3 nm), the slip effect induced by the interaction of the airflow stream around the periphery of adjacent nanofibers can be effectively utilized [1]. With effective control of the conductivity and viscosity of the polymer solution, the optimized electrospinning process and control of the PVDF polymer solution with SDS as an additive may achieve the desired morphology of the PVDF nanomembrane. As shown in Fig. 1b, the 15 wt% concentration of bare PVDF exhibits non-uniform large-diameter fibers in the range of 80–250 nm. These are mixed with an oval-shaped beaded structure that is five-fold larger than a typical fiber in the direction of the fiber length. The resultant beads on fibers may be attributed to the low viscosity of the polymer solution, which causes the imbalance between surface tension, electrostatic repulsion, and the instability of the Taylor cone at the spinneret tip [43]. The uncontrolled beaded structure may be

suppressed by increasing the polymer concentration to improve solution viscosity; however, it also induces a larger fiber diameter. However, it has been observed that modifying the polymer solution conductivity with ionic surfactant results in improved morphology uniformity and thinner-diameter fibers. This is owing to the decrease in the surface tension of the solution, which produces a greater Coulombic interaction and results in an improved stretchability of the electrospun liquid jet. Therefore, SDS was introduced to mitigate the surface tension and enhance charge density or solution conductivity [42,44].

Fig. 1b–d clearly exhibit the morphological transformation of electrospun NFs under the influence of different amounts of SDS surfactant. Specifically, the bead-containing fibers were gradually eliminated with increased SDS concentration (Fig. S1), and NF web uniformity was finally achieved. Moreover, as shown in Fig. 1b–c, the fiber diameter becomes substantially thinner with the addition of SDS. The SDS-free PVDF NF web exhibits the largest average diameter of approximately 250 nm, and the NF with 0.5 wt%-SDS has a very thin NF web of approximately 70 nm with the highest homogeneity, which is close to the aforementioned mean free path of the air molecules.

3.2. Chemical characterization of PVDF nanofibers

As shown in Fig. 2, FTIR and GIXRD measurements were taken to gain a comprehensive understanding of the PVDF polymorphs in the electrospun PVDF nanofibers. The FTIR spectra in Fig. 2a indicate the phase transformation of PVDF from the thermodynamically stable α phase of the powder sample to the ferroelectric β phase of the nano-confined electrospun nanofiber sample. The vibrational band of the α phase, located at 765 cm^{-1}, 855 cm^{-1}, and 976 cm^{-1} in the PVDF powder sample, gradually fades in the solution cast membrane and almost disappears at the electrospun nanofiber samples. The vibrational bands of the β phase, located at 840 cm^{-1} and 1279 cm^{-1}, present weak signals for the pristine PVDF powder; however, the bands become more visible in the solution cast membrane. The β vibrational mode is sharply enhanced in the electrospun nanofibers owing to the high electric force of the electrospinning system [45,46]. According to the absorbance values obtained from the FTIR measurement, the fraction of β phase among crystalline region (F(β)) can be quantitatively determined using the Beer–Lambert law by neglecting amorphous region with the following equation:

$$F(\beta) = \frac{X_\beta}{X_\alpha + X_\beta} = \frac{A_\beta}{\left(\frac{K_\beta}{K_\alpha}\right)A_\alpha + A_\beta} \tag{2}$$

X_α, X_β are the degree of crystallinity of α and β phases, respectively. Aα and A_β are the absorbance values of the α and β phases at 765 cm^{-1} and 840 cm^{-1}, respectively. K_α (6.1 ×10^4 cm^2/mol) and K_β (7.7 ×10^4 cm^2/mol) are the absorption coefficients at the corresponding wavenumbers. The ratio of $K_\beta/K_\alpha = 1.3$ is considered to be a constant for this Eq. (2) [47–49]. As shown in Table 1, the obtained F(β) values are considerably different to those of the samples before and after being processed by electrospinning. Specifically, while the PVDF powder with a dominant nonpolar α phase exhibits a poor F(β) of 39.42%, the solution cast thin film sample exhibits a F(β) of approximately 55%. The F(β) dramatically increases to 70.15% for the 250-nm electrospun fibers without the SDS surfactant, and it eventually reaches 87% for the 70-nm-fiber sample (with 0.5 wt% of SDS).

Additionally, the XRD diffraction peaks of the α(100) phase at 17.7° and β(110) phase at 20.26° in Fig. 2**b** confirm the phase change from α to β within the nanofibers [50,51]. In accordance with the FTIR results, the PVDF powder reflects three major XRD peak positions at 18.27°, 19.7°, 26.5°, and 33.2°, which are matched with the monoclinic α crystalline phase [45,52,53]. The clear phase transformation into the β phase is observed for the solution cast thin film and electrospun PVDF nanofiber. The calculated ratio of the β phase to α phase (A_β/A_α) in Fig. S2 and Table 1 indicates that the enhancement of the β diffraction peak can be
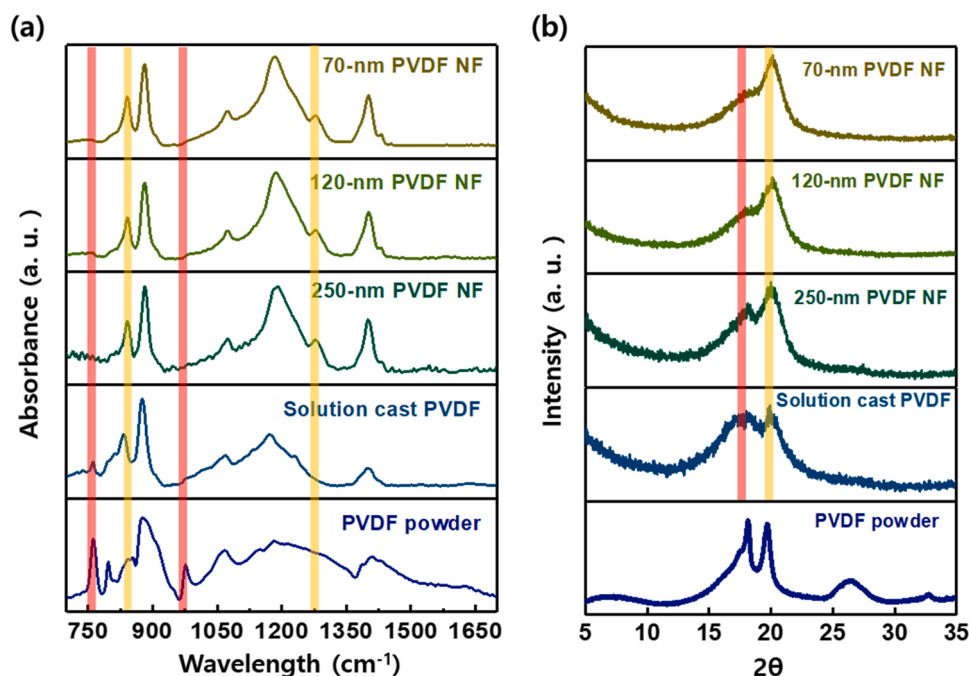
Fig. 2. Phase identification of PVDF nanofiber. (a) FT-IR spectra and (b) XRD patterns of PVDF at various forms and diameters.

Table 1
β phase fraction and the ratio of β phase versus α phase at various PVDF forms.

Sample	β fraction (%)	A_β/A_α
PVDF powder	39.42	–
Solution cast PVDF	54.62	0.44
250-nm PVDF NF	70.15	0.90
120-nm PVDF NF	83.70	1.42
70-nm PVDF NF	87.0	1.61

observed in accordance with the relative reduction of the nanofibrous diameter. The gradual displacement of the α phase by the β phase in 250-nm PVDF nanofibers may be induced by the poling effect of the PVDF chain by a large electric field during electrospinning. Moreover, the higher concentration of the β phase in the small-diameter samples is attributed to an enriched charge density from the addition of SDS and confinement with a small diameter. The charged polymer jets with a smaller diameter experience a more powerful stretching force associated with the applied high electric field, thereby facilitating the PVDF phase transition from the α phase to the β phase [54].

3.3. Local polarization switching in PVDF nanofibers by piezoresponse force microscopy

Piezoresponse force microscopy (PFM) is an advanced scanning probe microscopy (SPM) technique based on the strong coupling between polarization and electromechanical behavior. PFM measures the dynamic electromechanical response of the ferroelectric material when an ac voltage is applied to the SPM tip in mechanical contact with a sample surface [55]. Because of the inverse piezoelectric effect, the electric signal imposed on the SPM tip makes the ferroelectric material expand or contract at nanoscale. This is measured as cantilever deflection through a change in laser spot position on a photodetector in the SPM head unit. The ac component of the cantilever deflection is measured using lock-in techniques and then its amplitude and phase are used to determine the local piezoelectric strength and orientation of the ferroelectric domain. The PFM amplitude indicates the magnitude of the local electromechanical coupling, while the PFM phase affords the ferroelectric domain orientation. In particular, PFM hysteresis loops, in

which electromechanical response is measured as a function of applied dc bias, are used to determine the ferroelectricity of nanomaterials. It is generally accepted that the local PFM loops are good agreement with macroscopic polarization-electric field (P-E) measurements despite the fundamentally different mechanism in local and macroscopic switching [55]. From the 70-nm, 120-nm, and 250-nm PVDF NF membrane samples, topographic images of the PVDF nanofibers (diameters of 70 nm, 120 nm, and 200 nm) corresponding to the PFM measurements are shown in Fig. 3a–c, respectively. The PFM measurement setup and switching/probing waveforms are illustrated in Fig. 3d. To avoid non-hysteretic electrostatic contribution to the PFM signal, the piezoresponse was probed after the dc bias was turned off, yielding off-field hysteresis loop [56]. Local piezoelectric hysteresis loops of the PVDF nanofibers differently sized in diameters were recorded as a function of the applied dc bias voltage. The measured loops exhibited ferroelectric characteristics, butterfly amplitude (*A*) loops and 180° phase (*φ*) flips when the amplitude was at a minimum, as shown in Fig. 3e and f, respectively. In inorganic ferroelectric materials, electrostrictive deformation is much smaller than piezoelectric one and thus can be ignored. However, our PVDF nanofibers are semi-crystalline and the electrostriction resulting from amorphous and non-polar phases may not be ignored. The piezoelectric effect as an electrostriction biased by the polarization or linearized electrostriction can be expressed via the following equation:[57].

$$d_{eff} = 2Q_{eff}\epsilon_0\epsilon P \tag{3}$$

where $Q_{eff}(E)$ is an effective electrostriction coefficient, ϵ_0 is the permittivity of vacuum, ϵ is the relative dielectric permittivity, and *P* is the spontaneous polarization. The piezoresponse of ferroelectric phases was still dominant in the PFM hysteresis loop, but the electrostrictive deformation caused by amorphous and non-polar phases might allow for vertically shifting the butterfly amplitude loops (Fig. 3e). The asymmetry of the tip/nanofiber/Au configuration also resulted in the shift of both amplitude and phase loops along the voltage axis (Fig. 3e and f). Notably, only 70 nm diameter nanofibers showed excellent butterfly amplitude and square phase loops. The steep slope at a coercive voltage in the amplitude loop implies the large d_{33} value of the nanofiber [58]. These coincide with FTIR and XRD observations above.
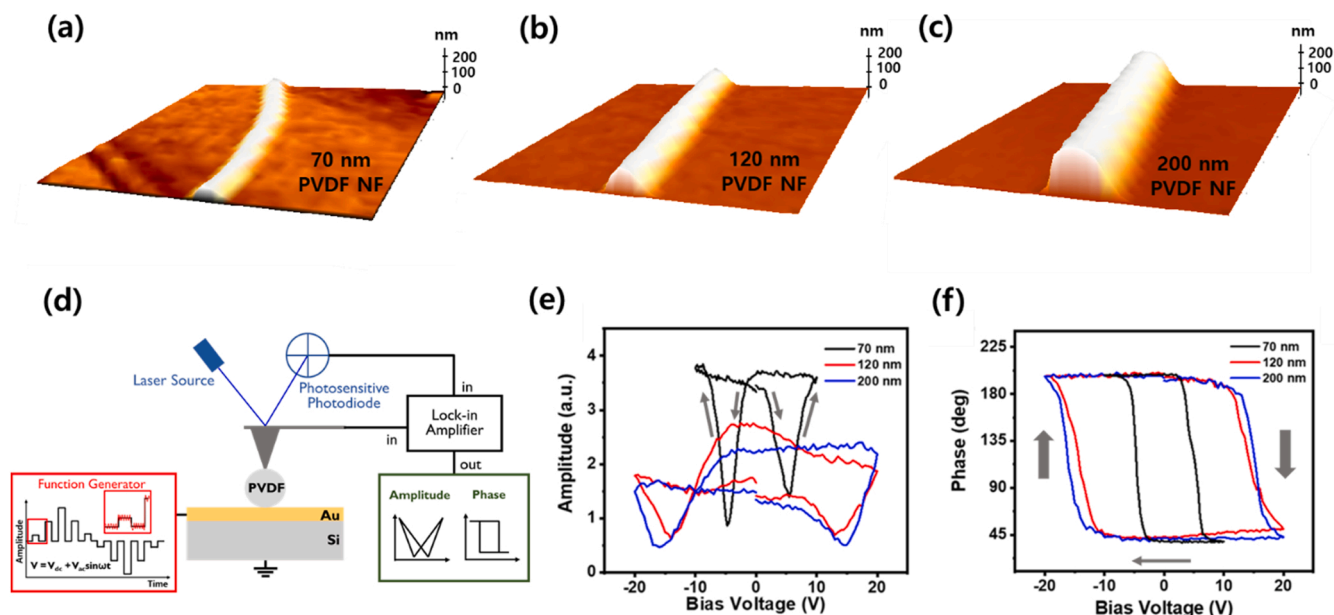
Fig. 3. Piezoresponse force microscopy measurement of PVDF NF. Topography images of PVDF NFs with a diameter of (a) 70 nm, (b) 120 nm and (c) 200 nm. (d) PFM measurement illustration. (e) Amplitude loop and (f) phase loop of PVDF NFs with diameter of 70 nm, 120 nm, and 200 nm.

3.4. Air filtration efficiency

The synergetic combination of ferroelectricity and the slip effect of ultrathin PVDF NFs can enhance the $PM_{0.3}$ capturing capability. Fig. 4a highlight the distinctive performance in filtering fine dust in various mass areas of 120-nm and 70-nm PVDF NF webs compared with the larger size (250 nm) of the SDS-free PVDF filter. Interestingly, the 250-nm PVDF NF filter has the lowest FE at the same loaded basis weight of the fibers. Despite an increase in the mass area of up to 2.5 g/m^2, the FE of the 250-nm PVDF NF filter is approximately 46.4% at a pressure drop of 30 Pa. This is clearly caused by the large fiber diameter and the negative effect of the beaded structure, which consumes a partial mass of the injected polymer. However, at the loaded basis weight of 0.25 g/m^2, the 120-nm PVDF NF membrane showed improvement in its FE of 74.65% with an equivalent pressure drop of 29 Pa. As clearly indicated in Fig. 4b, the most optimal performance was precisely achieved at the 70-nm fibrous membrane, with an air-FE of 97.387% and a pressure drop of 51 Pa accompanied by QF = 0.07 Pa^{-1} at the loaded mass area of 0.125 g/m^2. Further decrease of nanofiber mass area can result in higher quality factor due to the drastic reduction of pressure drop [59], which is shown in Fig. S3. As confirmed via spectroscopy and piezoelectric force microscopy, the largest ferroelectricity of the 70-nm PVDF

nanofiber may be highly effective in the $PM_{0.3}$ capture of the nanofiber membrane and subsequent enhancement of air FE. It has been reported that the remnant polarization of ferroelectricity results in an enhanced electrostatic interaction of filter membrane which is beneficial for micro-dust capture [37,60]. As previously mentioned, the 70 nm diameter is close to the mean free path of air molecules, which enables them to bypass the thin nanofibers and results in a significant decrease in pressure encountered by the air stream and filter membrane.

To evaluate the $PM_{0.3}$ filtration performance enhancement of PVDF NF with a smaller diameter, the three representative nanofibrous diameter membranes were fabricated at a similar pressure drop at approximately 30–31 Pa. Fig. 4c shows the measured FE and equivalent QF, which exhibit a clear increase with a nanofibrous diameter reduction. As the nanofibrous diameter reaches 70 nm, the filter displays the highest FE of 90.1% and the highest QF of 0.075 Pa^{-1} with a relative pressure drop of 31 Pa. Moreover, Fig. S4 and Table S1 show the obvious impact of the ultrathin PVDF NF filter membrane on $PM_{0.3}$ air filtration when compared with previously reported NF membranes. Although some complicated nanostructure-based membranes could exhibit better air filtration performance, the complicated structure could hinder the large-scale industrial implementation of NF membrane. Fig. S4a shows the uniform 70 nm-PVDF NF filter as indicated by the lowest basis
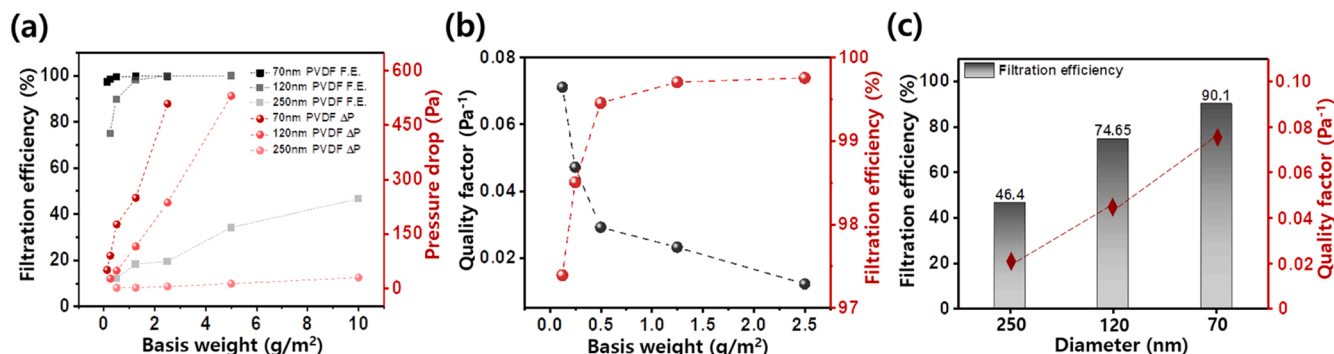
Fig. 4. Air filtration efficiency performance of nanofibrous filters. (a) The air filtration efficiency and pressure drop of representative 250-nm PVDF NF, 120-nm PVDF NF and 70-nm PVDF NF filters. (b) The QF and air filtration efficiency of 70-nm PVDF NF based air filter membrane. (c) The QF and air filtration efficiency of representative 250-nm, 120-nm, and 70-nm PVDF NF filters with a pressure drop of 30–31 Pa.

weight of 0.5 g/m² and a competitive FE of 99.45%. Among homogeneous NF membranes, Fig. S4b clearly exhibits the significantly low pressure drop of ultrathin PVDF nanofiber filter compared to the other materials. Fig. S4c–d and Table S2 compare the filtration performance of the simple nanofiber-based filter membranes, which are suitable to industrial scalability. The ferroelectric PVDF nanofiber web stands out as a strong candidate with a low air resistance and high $PM_{0.3}$ capturing efficiency.

3.5. Chemical and thermal stability

The superior chemical and thermal stabilities of the electrospun PVDF NF filter were investigated by immersing the 70-nm fibers in an IPA bath for various time periods and annealing for 24 h at 40–120 °C under ambient air in an oven, respectively. Fig. 5a shows the superior FE of the PVDF nanofibrous membrane against polypropylene (PP) MB filters. Specifically, the PP MB membranes show a rapid decay of FE, from 99.91% to nearly 35%, after 15 min of immersion in IPA. The significant FE degradation is undoubtedly attributed to the charge loss of the PP MB filter by IPA penetration into the polymer matrix [26]. In contrast, the PVDF nanofibrous membrane (FE = 94.901%, ΔP = 45 Pa) exhibits a high filtration performance retention of 92.63% (FE = 87.903%, ΔP = 65 Pa) after 60 min of immersion in IPA. As shown in Fig. 5b–c, the slight decrease in FE is owing to the degradation of the general crystalline phases of the PVDF nanofiber by solvent impregnation and subsequent ferroelectric β phase loss or dipole moment loss [61]. However, the 81.21% FE retention of the PVDF NF filter after an 8 h immersion in IPA, as shown in Fig. S5a, clearly confirms the superior chemical stability of the PVDF NF filter compared with the stability of the PP MB filter.

For thermal stability, Fig. 5d shows the excellent filtration performance of the PVDF nanofibrous membrane under a high temperature treatment with an insignificant FE decrease (ΔFE = 1.89%) at 100 °C. Interestingly, the 120 °C treated sample exhibited an improved filter performance up to an FE of 95.99% and QF of 0.057 Pa⁻¹. As shown in Figs. 5e–f and S5b–c, the major vibrational bands from the FTIR spectra and the crystalline peaks from the XRD patterns of the β phase remain nearly unchanged under a high temperature treatment. The increasing behavior from a sample treated at 120 °C can be explained by the increase in the β phase vibrational bands in Fig. 5e and the XRD patterns in Fig. 5f, which have a slightly sharper β phase peak at 120 °C and exhibit a gradual disappearance of the characteristic α phase. As reported in previous studies, the annealing treatment can induce a phase transformation from the nonpolar α phase to the polar β phase owing to the reorientation of the PVDF molecular structure. This leads to a reordering of dipole moments, thereby sharpening the crystalline peak of the β phase and subsequent intense ferroelectricity at higher annealing temperatures [39,62]. Prolonged heating treatment at high temperature might result in the filtration performance degradation due to the slight deterioration of PVDF crystalline phases consisting of β phase [63], which is clearly depicted by XRD patterns in Fig. S6.

4. Conclusions

The ferroelectric PVDF nanofiber membrane for a $PM_{0.3}$ filter was successfully fabricated with the introduction of SDS surfactant. With a high fraction of the β phase (87%), the 70-nm PVDF nanofibrous membrane from the solution that contained 0.5% SDS exhibited a clear phase polarization with the largest piezoelectric deformation. Under the synergetic combination of the slip and ferroelectric effects, the 70-nm PVDF filter membrane exhibited a high $PM_{0.3}$ FE of 97.4%, a low pressure drop of 51 Pa, and a high QF of 0.07 Pa⁻¹. Notably, the high-performance ultrathin 70-nm PVDF membrane also possesses excellent chemical and thermal stability with high retention of air FE under
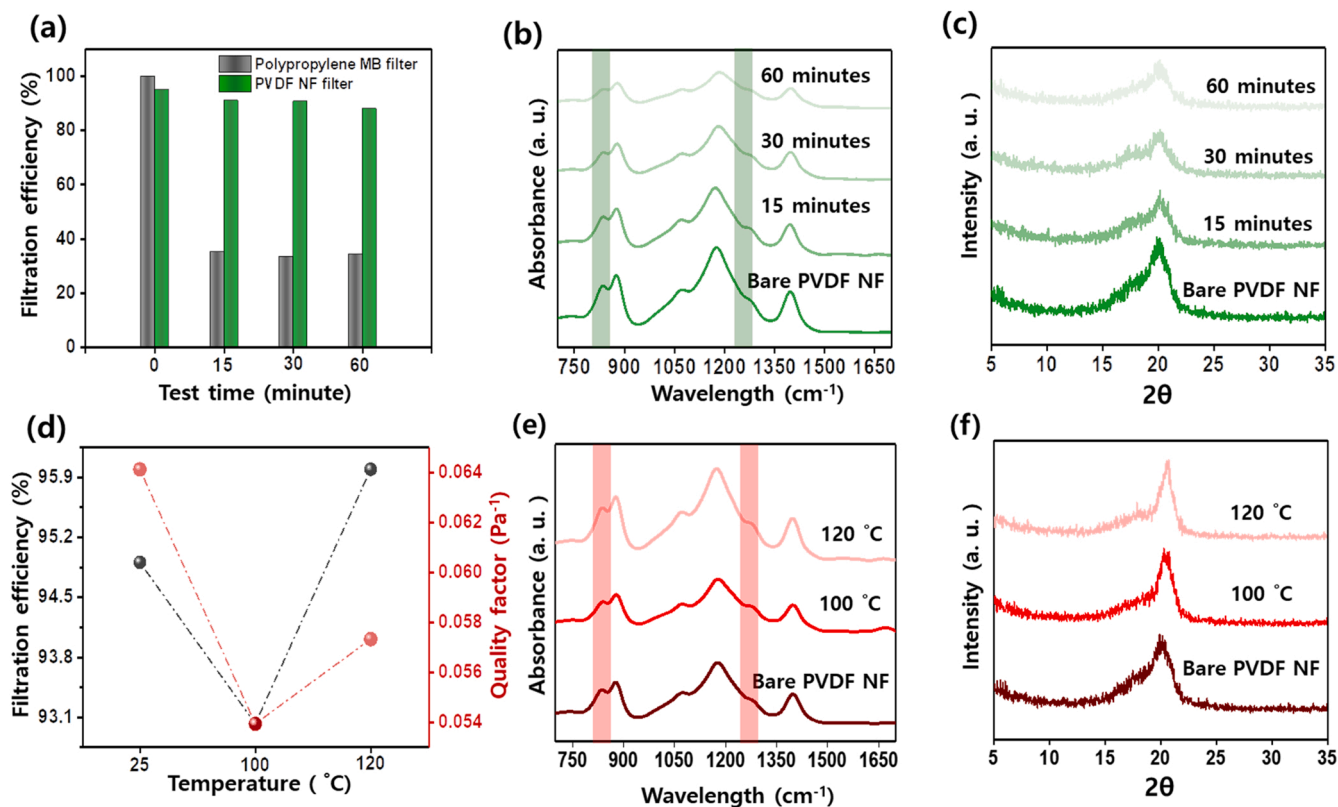
Fig. 5. Chemical and thermal stability of a PVDF nanofibrous membrane. (a) Filtration efficiency comparison of PVDF nanofibrous membrane and PP MB membrane after IPA treatment. (b) FTIR and (c) XRD of PVDF nanofiber immersed in IPA for various time periods. (d) Filtration performance of PVDF nanofibrous membrane after high temperature treatment. (e) FTIR and (f) XRD of PVDF nanofiber heated at various temperatures for 24 h.

various treatment conditions. Thus, we conclude that the ferroelectric PVDF NF filter is an outstanding candidate to mitigate microdust pollutants and temporary COVID-19 prevention problems.

CRediT authorship contribution statement

Tan Tan Bui: Conceptualization, Investigation, Data curation, Writing – original draft. **Min Kyoung Shin**: Investigation, Data curation. **Seung Yong Jee**: Resources, Investigation, Data curation. **Dang Xuan Long**: Investigation, Data curation. **Jongin Hong**: Data curation, Supervision, Writing – original draft, Writing – review & editing, Funding acquisition. **Myung-Gil Kim**: Conceptualization, Data curation, Supervision, Writing – original draft, Writing – review & editing, Funding acquisition.

Declaration of Competing Interest

The authors declare that they have no known competing financial interests or personal relationships that could have appeared to influence the work reported in this paper.

Acknowledgments

Appendix A. Supporting information

Supplementary data associated with this article can be found in the online version at doi:10.1016/j.colsurfa.2022.128418.

References

[1] X. Zhao, S. Wang, X. Yin, J. Yu, B. Ding, Slip-effect functional air filter for efficient purification of PM2.5, Sci. Rep. 6 (2016) 1–11.
[2] K.-H. Kim, E. Kabir, S. Kabir, A review on the human health impact of airborne particulate matter, Environ. Int. 74 (2015) 136–143.
[3] K. Lee, B. Liu, On the minimum efficiency and the most penetrating particle size for fibrous filters, J. Air Pollut. Control Assoc. 30 (1980) 377–381.
[4] K.-S. Lee, N. Hasolli, S.-M. Jeon, J.-R. Lee, K.-D. Kim, Y.-O. Park, J. Hwang, Filter layer structure effect on the most penetrating particle size of multilayered flat sheet filter, Powder Technol. 344 (2019) 270–277.
[5] C.H. Jung, H.-S. Park, Y.P. Kim, Theoretical study for the most penetrating particle size of dust-loaded fiber filters, Sep. Purif. Technol. 116 (2013) 248–252.
[6] A. Podgorski, A. Bałazy, L. Gradoń, Application of nanofibers to improve the filtration efficiency of the most penetrating aerosol particles in fibrous filters, Chem. Eng. Sci. 61 (2006) 6804–6815.
[7] H.-C. Wang, G. Kasper, Filtration efficiency of nanometer-size aerosol particles, J. Aerosol Sci. 22 (1991) 31–41.
[8] J.D. Sacks, L.W. Stanek, T.J. Luben, D.O. Johns, B.J. Buckley, J.S. Brown, M. Ross, Particulate matter–induced health effects: who is susceptible? Environ. Health Perspect. 119 (2011) 446–454.
[9] C.J. Lee, R.V. Martin, D.K. Henze, M. Brauer, A. Cohen, Av Donkelaar, Response of global particulate-matter-related mortality to changes in local precursor emissions, Environ. Sci. Technol. 49 (2015) 4335–4344.
[10] G.B. Hamra, N. Guha, A. Cohen, F. Laden, O. Raaschou-Nielsen, J.M. Samet, P. Vineis, F. Forastiere, P. Saldiva, T. Yorifuji, Outdoor particulate matter exposure and lung cancer: a systematic review and meta-analysis, Environ. Health Perspect. 122 (2014) 906.
[11] P. Cui, Y. Huang, J. Han, F. Song, K. Chen, Ambient particulate matter and lung cancer incidence and mortality: a meta-analysis of prospective studies, Eur. J. Public Health 25 (2015) 324–329.
[12] S. Zhang, H. Liu, N. Tang, S. Zhou, J. Yu, B. Ding, Spider-web-inspired PM0.3 filters based on self-sustained electrostatic nanostructured networks, Adv. Mater. 32 (2020) 2002361.
[13] F. Wu, S. Zhao, B. Yu, Y.-M. Chen, W. Wang, Z.-G. Song, Y. Hu, Z.-W. Tao, J.-H. Tian, Y.-Y. Pei, A new coronavirus associated with human respiratory disease in China, Nature 579 (2020) 265–269.
[14] C. Huang, Y. Wang, X. Li, L. Ren, J. Zhao, Y. Hu, L. Zhang, G. Fan, J. Xu, X. Gu, Clinical features of patients infected with 2019 novel coronavirus in Wuhan, China, Lancet 395 (2020) 497–506.
[15] R. Verity, L.C. Okell, I. Dorigatti, P. Winskill, C. Whittaker, N. Imai, G. Cuomo-Dannenburg, H. Thompson, P.G. Walker, H. Fu, Estimates of the severity of coronavirus disease 2019: a model-based analysis, Lancet Infect. Dis. 20 (2020) 669.
[16] Q. Zhang, J. Welch, H. Park, C.-Y. Wu, W. Sigmund, J.C. Marijnissen, Improvement in nanofiber filtration by multiple thin layers of nanofiber mats, J. Aerosol Sci. 41 (2010) 230–236.
[17] K.M. Yun, C.J. Hogan Jr, Y. Matsubayashi, M. Kawabe, F. Iskandar, K. Okuyama, Nanoparticle filtration by electrospun polymer fibers, Chem. Eng. Sci. 62 (2007) 4751–4759.
[18] Y. Lee, L.C. Wadsworth, Structure and filtration properties of melt blown polypropylene webs, Polym. Eng. Sci. 30 (1990) 1413–1419.
[19] R.D. Anandjiwala, L. Boguslavsky, Development of needle-punched nonwoven fabrics from flax fibers for air filtration applications, Text. Res. J. 78 (2008) 614–624.
[20] L. Xia, Q. Zhang, X. Zhuang, S. Zhang, C. Duan, X. Wang, B. Cheng, Hot-pressed wet-laid polyethylene terephthalate nonwoven as support for separation membranes, Polymers 11 (2019) 1547.
[21] Z. Wang, C. Zhao, Z. Pan, Porous bead-on-string poly(lactic acid) fibrous membranes for air filtration, J. Colloid Interface Sci. 441 (2015) 121–129.
[22] X. Li, N. Wang, G. Fan, J. Yu, J. Gao, G. Sun, B. Ding, Electreted polyetherimide–silica fibrous membranes for enhanced filtration of fine particles, J. Colloid Interface Sci. 439 (2015) 12–20.
[23] R.-R. Cai, S.-Z. Li, L.-Z. Zhang, Y. Lei, Fabrication and performance of a stable micro/nano composite electret filter for effective PM2.5 capture, Sci. Total Environ. 725 (2020), 138297.
[24] H. Zhang, J. Liu, X. Zhang, C. Huang, X. Jin, Design of electret polypropylene melt blown air filtration material containing nucleating agent for effective PM2.5 capture, RSC Adv. 8 (2018) 7932–7941.
[25] S. Wang, X. Zhao, X. Yin, J. Yu, B. Ding, Electret polyvinylidene fluoride nanofibers hybridized by polytetrafluoroethylene nanoparticles for high-efficiency air filtration, ACS Appl. Mater. Interfaces 8 (2016) 23985–23994.
[26] H. Xiao, Y. Song, G. Chen, Correlation between charge decay and solvent effect for melt-blown polypropylene electret filter fabrics, J. Electrost. 72 (2014) 311–314.
[27] J. Kim, J.P. Hinestroza, W. Jasper, R. Barker, Effect of solvent exposure on the filtration performance of electrostatically charged polypropylene filter media, Text. Res. J. 79 (2009) 343–350.
[28] H.-J. Choi, E.-S. Park, J.-U. Kim, S.H. Kim, M.-H. Lee, Experimental study on charge decay of electret filter due to organic solvent exposure, Aerosol Sci. Technol. 49 (2015) 977–983.
[29] S. Ullah, A. Ullah, J. Lee, Y. Jeong, M. Hashmi, C. Zhu, K.I. Joo, H.J. Cha, I.S. Kim, Reusability comparison of melt-blown vs nanofiber face mask filters for use in the coronavirus pandemic, ACS Appl. Nano Mater. 3 (2020) 7231–7241.
[30] H. Li, Z. Wang, H. Zhang, Z. Pan, Nanoporous PLA/(chitosan nanoparticle) composite fibrous membranes with excellent air filtration and antibacterial performance, Polymers 10 (2018) 1085.
[31] L. Gradoń, Influence of electrostatic interactions and slip effect on aerosol filtration efficiency in fiber filters, Ind. Eng. Chem. Res. 26 (1987) 306–311.
[32] L. Bao, K. Seki, H. Niinuma, Y. Otani, R. Balgis, T. Ogi, L. Gradoń, K. Okuyama, Verification of slip flow in nanofiber filter media through pressure drop measurement at low-pressure conditions, Sep. Purif. Technol. 159 (2016) 100–107.
[33] J. Doshi, D.H. Reneker, Electrospinning process and applications of electrospun fibers, J. Electrost. 35 (1995) 151–160.
[34] S.-H. Tan, R. Inai, M. Kotaki, S. Ramakrishna, Systematic parameter study for ultra-fine fiber fabrication via electrospinning process, Polymer 46 (2005) 6128–6134.
[35] W.E. Teo, S. Ramakrishna, A review on electrospinning design and nanofibre assemblies, Nanotechnology 17 (2006) R89.
[36] H.-J. Kim, S.J. Park, C.S. Park, T.-H. Le, S.H. Lee, T.H. Ha, H.-i Kim, J. Kim, C.-S. Lee, H. Yoon, Surface-modified polymer nanofiber membrane for high-efficiency microdust capturing, Chem. Eng. J. 339 (2018) 204–213.
[37] D. Park, M. Kim, S. Lee, I.J. Yoon, K. Lee, M.H. Lee, J. Nah, Light-permeable air filter with self-polarized nylon-11 nanofibers for enhanced trapping of particulate matters, Adv. Mater. Interfaces 6 (2019) 1801832.
[38] L. Ruan, X. Yao, Y. Chang, L. Zhou, G. Qin, X. Zhang, Properties and applications of the β phase poly(vinylidene fluoride), Polymers 10 (2018) 228.
[39] R. Gregorio Jr, Determination of the α, β, and γ crystalline phases of poly (vinylidene fluoride) films prepared at different conditions, J. Appl. Polym. Sci. 100 (2006) 3272–3279.
[40] M. Alaaeddin, S. Sapuan, M. Zuhri, E. Zainudin, F.M. AL-Oqla, Properties and common industrial applications of polyvinyl fluoride (PVF) and polyvinylidene fluoride (PVDF), IOP Conf. Ser.: Mater. Sci. Eng. 409 (2018), 012021.
[41] X. Chen, X. Han, Q.D. Shen, PVDF-based ferroelectric polymers in modern flexible electronics, Adv. Electron. Mater. 3 (2017) 1600460.
[42] N. Soin, D. Boyer, K. Prashanthi, S. Sharma, A.A. Narasimulu, J. Luo, T.H. Shah, E. Siores, T. Thundat, Exclusive self-aligned β-phase PVDF films with abnormal piezoelectric coefficient prepared via phase inversion, Chem. Commun. 51 (2015) 8257–8260.
[43] T. Lin, H. Wang, H. Wang, X. Wang, The charge effect of cationic surfactants on the elimination of fibre beads in the electrospinning of polystyrene, Nanotechnology 15 (2004) 1375.
[44] J.-Y. Zheng, M.-F. Zhuang, Z.-J. Yu, G.-F. Zheng, Y. Zhao, H. Wang, D.-H. Sun, The effect of surfactants on the diameter and morphology of electrospun ultrafine nanofiber, J. Nanomater. 2014 (2014), 689298.
[45] X. Li, C. Wang, X. Huang, T. Zhang, X. Wang, M. Min, L. Wang, H. Huang, B. S. Hsiao, Anionic surfactant-triggered steiner geometrical poly(vinylidene fluoride) nanofiber/nanonet air filter for efficient particulate matter removal, ACS Appl. Mater. Interfaces 10 (2018) 42891–42904.

[46] E.S. Cozza, O. Monticelli, E. Marsano, P. Cebe, On the electrospinning of PVDF: influence of the experimental conditions on the nanofiber properties, Polym. Int. 62 (2013) 41–48.

[47] J. Gregorio, Rinaldo, M. Cestari, Effect of crystallization temperature on the crystalline phase content and morphology of poly(vinylidene fluoride), J. Polym. Sci. B Polym. Phys. 32 (1994) 859–870.

[48] P. Thakur, A. Kool, B. Bagchi, N.A. Hoque, S. Das, P. Nandy, In situ synthesis of Ni (OH)2 nanobelt modified electroactive poly(vinylidene fluoride) thin films: remarkable improvement in dielectric properties, Phys. Chem. Chem. Phys. 17 (2015) 13082–13091.

[49] P. Martins, A. Lopes, S. Lanceros-Mendez, Electroactive phases of poly(vinylidene fluoride): determination, processing and applications, Prog. Polym. Sci. 39 (2014) 683–706.

[50] G. Davis, J. McKinney, M. Broadhurst, S. Roth, Electric-field-induced phase changes in poly(vinylidene fluoride), J. Appl. Phys. 49 (1978) 4998–5002.

[51] W. Li, Q. Meng, Y. Zheng, Z. Zhang, W. Xia, Z. Xu, Electric energy storage properties of poly(vinylidene fluoride), Appl. Phys. Lett. 96 (2010), 192905.

[52] S. Janakiraman, A. Surendran, S. Ghosh, S. Anandhan, A. Venimadhav, Electroactive poly(vinylidene fluoride) fluoride separator for sodium ion battery with high coulombic efficiency, Solid State Ion. 292 (2016) 130–135.

[53] S. Janakiraman, A. Surendran, R. Biswal, S. Ghosh, S. Anandhan, A. Venimadhav, Electrospun electroactive polyvinylidene fluoride-based fibrous polymer electrolyte for sodium ion batteries, Mater. Res. Express 6 (2019), 086318.

[54] S. Sharafkhani, M. Kokabi, High performance flexible actuator: PVDF nanofibers incorporated with axially aligned carbon nanotubes, Compos. B. Eng. 222 (2021), 109060.

[55] S.V. Kalinin, A.N. Morozovska, L.Q. Chen, B.J. Rodriguez, Local polarization dynamics in ferroelectric materials, Rep. Prog. Phys. 73 (2010), 056502.

[56] N. Balke, P. Maksymovych, S. Jesse, A. Herklotz, A. Tselev, C.B. Eom, I. I. Kravchenko, P. Yu, S.V. Kalinin, Differentiating ferroelectric and nonferroelectric electromechanical effects with scanning probe microscopy, ACS Nano 9 (2015) 6484–6492.

[57] A.L. Kholkin, E.K. Akdogan, A. Safari, P.F. Chauvy, N. Setter, Characterization of the effective electrostriction coefficients in ferroelectric thin films, J. Appl. Phys. 89 (2001) 8066–8073.

[58] X. Liu, S. Xu, X. Kuang, D. Tan, X. Wang, Nanoscale investigations on β-phase orientation, piezoelectric response, and polarization direction of electrospun PVDF nanofibers, RSC Adv. 6 (2016) 109061–109066.

[59] J. Moon, T.T. Bui, S. Jang, S. Ji, J.T. Park, M.-G. Kim, A highly efficient nanofibrous air filter membrane fabricated using electrospun amphiphilic PVDF-g-POEM double comb copolymer, Sep. Purif. Technol. 270 (2021), 119625.

[60] K.S. Han, S. Lee, M. Kim, P. Park, M.H. Lee, J. Nah, Electrically activated ultrathin PVDF-TrFE air filter for high-efficiency PM1.0 filtration, Adv. Funct. Mater. 29 (2019) 1903633.

[61] R. Richards, The phase equilibria between a crystalline polymer and solvents, Trans. Faraday Soc. 42 (1946) 10–28.

[62] M. Satthiyaraju, T. Ramesh, Effect of annealing treatment on PVDF nanofibers for mechanical energy harvesting applications, Mater. Res. Express 6 (2019), 105366.

[63] P.J. Ratri, K. Tashiro, Phase-transition behavior of a crystalline polymer near the melting point: case studies of the ferroelectric phase transition of poly(vinylidene fluoride) and the β-to-α transition of trans-1,4-polyisoprene, Polym. J. 45 (2013) 1107–1114.